

Microstructural Characterization of Bonding Interfaces in Aluminum 3003 Blocks Fabricated by Ultrasonic Additive Manufacturing

A look at linking microstructure and linear weld density to the mechanical properties of ultrasonic additive manufacturing builds as well as analyzing their properties with different microscopy and testing methods

BY D. E. SCHICK, R. M. HAHNLEN, R. DEHOFF, P. COLLINS, S. S. BABU, M. J. DAPINO, AND J. C. LIPPOLD

ABSTRACT

Ultrasonic additive manufacturing (UAM) is a process by which hybrid and near-net-shaped products can be manufactured from thin metallic tapes. One of the main concerns of UAM is the development of anisotropic mechanical properties. In this work, the microstructures in the bond regions are characterized with optical and electron microscopy. Recrystallization and grain growth across the interface are proposed as a mechanism for the bond formation. The presence of voids or unbonded areas, which reduce the load-bearing cross section and create a stress intensity factor, is attributed to the transfer of the sonotrode texture to the new foil layer. This results in large peaks and valleys that are not filled in during processing. Tensile testing revealed the weld interface strength was 15% of the bulk foil. Shear tests of the weld interfaces showed almost 50% of the bulk shear strength of the material. Finally, optical microscopy of the fracture surfaces from the tensile tests revealed 34% of the interface area was unbonded.

Introduction

Ultrasonic additive manufacturing (UAM) is a solid-state joining process in which thin metallic tapes are ultrasonically welded on top of one another and periodically machined to create a final part. A schematic illustration of the process is shown in Fig. 1. Along with progressive building of a block through seam welding (Fig. 1A), a milling process (Fig. 1B) is used as required to create holes or channels before welding the subsequent layers. The machining operation is also used periodically to produce a flat surface to ensure proper dimensions of the finished build. This process offers many benefits over tra-

ditional fusion welding processes such as allowing for complex shapes and designs, having a significantly lower processing temperature, allowing for embedded materials and channels, and offering the capability of joining dissimilar materials that are otherwise difficult or impossible due to UAM being a solid-state process.

The majority of research on UAM is currently focused on optimizing processing parameters (Refs. 1–6) and characterizing the quality and microstructure (Refs. 7–9) of the resulting builds. The four main parameters in UAM are sonotrode amplitude,

travel speed, normal force applied, and preheat temperature. Increasing the amplitude, normal force, and preheat temperature, while decreasing the travel speed, generally increases the quality of the bonds. However, above a threshold for each parameter, no further gains are realized (Ref. 5). The threshold effects with respect to sonotrode amplitude and normal force are most likely due to the machine not being capable of delivering enough power to sustain the ultrasonic vibrations at the higher amplitudes and forces. Additional gains in bond quality may be possible with a higher-power system, allowing for higher amplitudes of vibration and forces. For most current UAM machines, optimum parameters are approximately 18–21 μm amplitude, 25–50 mm/s travel speed, preheat of 65°–150°C, and normal forces between 800 and 1500 N. Peel tests (Refs. 1, 2, 4, 6), fiber push-out testing (Ref. 3), and microhardness and nanohardness tests (Refs. 2, 9, 10) have been conducted to further the understanding of this additive manufacturing process. These tests are often done along with parameter development to compare the bond quality between different builds. Voids are often present in UAM builds and can be quantified with linear weld density (LWD). The LWD is defined as the length of a particular interface that appears properly bonded divided by the total interface length inspected. The LWD is often used as a test to determine optimum processing parameters (Refs. 1, 2, 4, 5, 11). It is generally agreed that to improve the bond quality of UAM builds, LWD must be kept as high as possible. In most UAM builds, LWD density ranges from 40 to 95%. Ram et al. (Ref. 5) and Johnson (Ref. 7) theorized voids form in UAM builds due to the sonotrode transferring its texture to the workpiece. This results in a situation where the top of each interface is smooth, but the bottom is

D. E. SCHICK, S. S. BABU (babu.13@osu.edu), and J. C. LIPPOLD are with the Department of Materials Science and Engineering — Welding Engineering Program, and R. M. HAHNLEN and M. J. DAPINO are with the Department of Mechanical Engineering at The Ohio State University, Columbus, Ohio. R. DEHOFF, formerly at the Department of Materials Science and Engineering, is currently at Oak Ridge National Laboratory, Oak Ridge, Tenn. P. COLLINS, formerly at the Department of Materials Science and Engineering, is currently at Quad Cities Manufacturing Laboratory, Rock Island, Ill.

KEYWORDS

Ultrasonic Additive Manufacturing (UAM)
Linear Weld Density (LWD)
Scanning Electron Microscopy (SEM)
Shear Strength
Al 3003-H18
Transmission Electron Microscopy

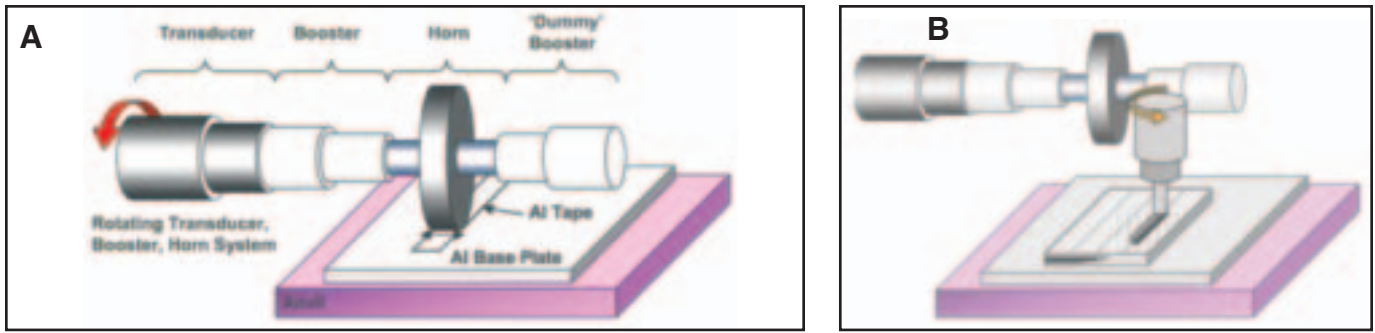


Fig. 1 — Schematic illustration of the UAM process. A — Adding a new tape layer; B — periodic milling operation to form final dimensions.

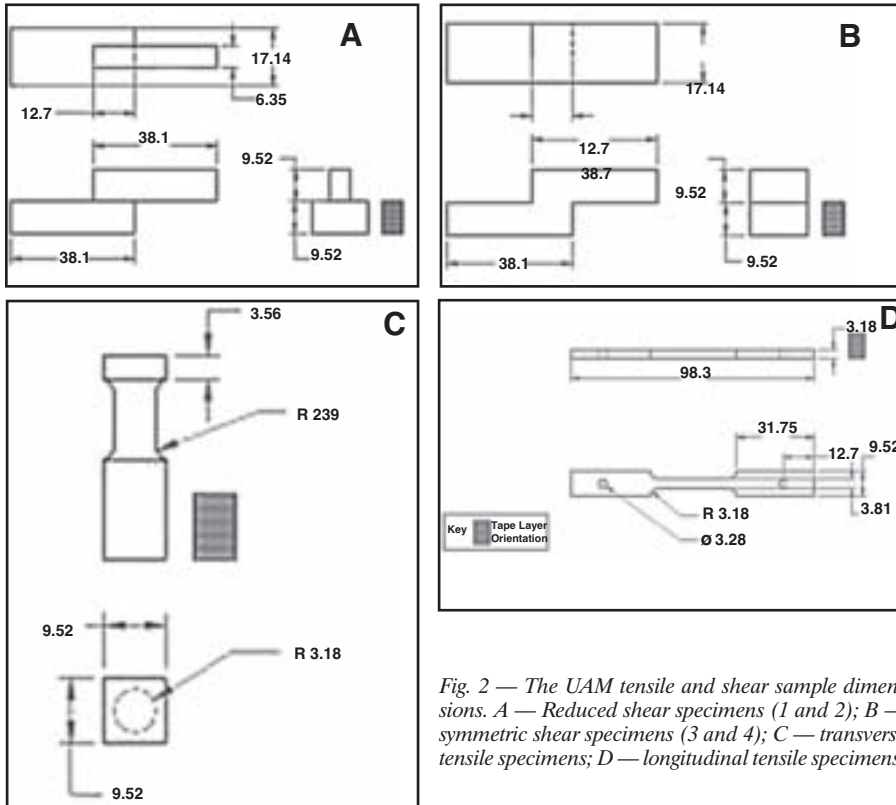


Fig. 2 — The UAM tensile and shear sample dimensions. A — Reduced shear specimens (1 and 2); B — symmetric shear specimens (3 and 4); C — transverse tensile specimens; D — longitudinal tensile specimens.

rough. To combat this, it has been demonstrated that milling between layer deposits to provide a smooth-to-smooth interface can eliminate voids, achieving 98% LWD (Ref. 5). However, no tensile, peel, or other quantitative measurement of bond quality was done to verify the bond quality.

Several researchers have made preliminary attempts at mechanical and finite element modeling (FEM) of UAM weldments. Doumanidis and Gao (Ref. 10) used an analytical model combined with experimental data to produce an FEM of

UAM useful in simulating different material combinations, embedding of materials, and the production of complex parts. This model also proved useful in determining ideal geometry for the sonotrode and other components. Zhang et al. (Ref. 12) developed a three-dimensional FEM for ultrasonic spot welding that evaluated the ever-changing parameters at each node including normal stress, heat generation, and plastic deformation. Their model used thermal and mechanical conditions to simulate the ultrasonic welding

process and led to the theory that ultrasonic bonds are formed due to high levels of localized strain, high temperatures, and plastic deformation along the interface. Siddiq et al. (Ref. 13) also developed a three-dimensional model focusing on friction and heat generation at the interface. Their simulation determined the effect of friction at the interface to be only useful in removing oxides and contaminants while the plastic deformation of material actually leads to a bond.

Multiple material combinations have been studied, including aluminum, copper, titanium, and nickel (Refs. 11, 13, 14), as well as many different fibers have been successfully embedded including fiber optics, silicon carbides, shape memory alloys, and thermocouples (Refs. 3, 6, 9, 11, 15, 16). The UAM process has been found to easily accommodate these embedded fibers as the ultrasonic energy allows for excellent matrix material flow around the fiber.

In all the above work, a one-to-one correlation of tensile and shear properties with the underlying microstructure has not been documented. Therefore, in this work, the mechanical properties of aluminum builds were measured and observed properties were correlated with the detailed microstructure evaluation using optical microscopy, hardness mapping, and electron microscopy. The results will be compared with published literature on UAM processes as well as data from ultrasonic spot welding. The methodology and data generated in this research are expected to provide a baseline for the development of a very high power UAM (VHP-UAM) instrument (Ref. 17). This instrument will be capable of joining higher-strength alloys including titanium, copper, nickel, shape memory alloys, carbon steels, and low-alloy steels.

Table 1 — UAM Processing Parameters Used in the Current Research

ID	Force (N)	Speed (mm/s)	Amplitude (µm)	Frequency (kHz)	Build Temperature (°C)
Tack	350	59.3	12	20	150
Weld	1150	42.3	17	20	150

Experimentation

Alloys

In this research, a non age-hardenable Al-3003 (Al-1Mn-0.7Fe-0.12Cu wt-%)

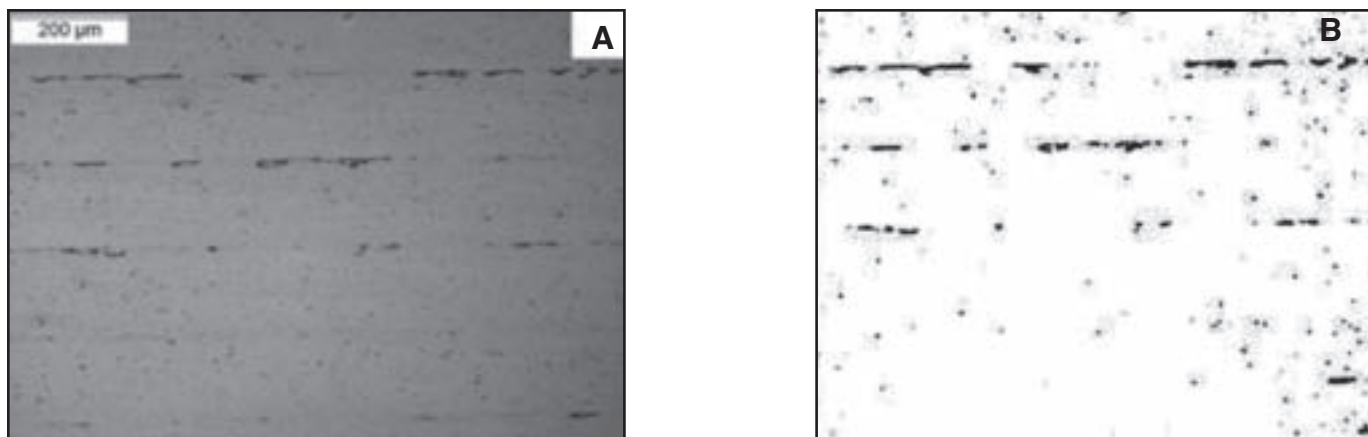


Fig. 3 — Sample image to demonstrate methodology used for image analyses to derive the linear weld density. A — Original optical microscopy image; B — processed image using ImageJ software.

alloy was used as both tapes (H18, 150 μm thick, 25.4 mm wide) and substrate (H14, more than 12.7 mm thick). The composition of the materials used meets the standard specification of the alloy (Ref. 18).

UAM Process Parameters

The ultrasonic sonotrode was made from Ti-6Al-4V alloy, and the surface was subjected to electrical discharge machining (EDM) to achieve the desired surface texture ($R_a = 7 \mu\text{m}$). This surface texture is known to provide consistent bond quality (Refs. 5, 7). During the tacking and welding passes, the substrate was preheated with a hot plate to 149°C (300°F) and was maintained at that temperature. The preheat was used to soften the material, which leads to better bonding. However, during processing, the tape and interface temperatures are not necessarily maintained at this preheat temperature due to complex heat transfer across the many weld interfaces, heat generated at the interfaces, and a heat-sinking effect due to the sonotrode.

Sequential joining of tapes to build a small block was achieved through tacking and welding passes. The differences between the tacking and welding passes are related to the magnitude of the process parameters, i.e., normal load, travel speed, and amplitude of ultrasonic vibration. In the current research, the vibration frequency was kept constant at 20 kHz for all passes due to machine and sonotrode design. Table 1 provides an overview of the processing parameters used in the current research. These processing parameters were obtained by extensive trial and error experiments. One method of testing process parameters involves joining of tapes by different process parameters and manually peel testing the builds. The best processing parameters are qualitatively selected when the manual peel test fractures the tape, rather than peeling off from the interfacial

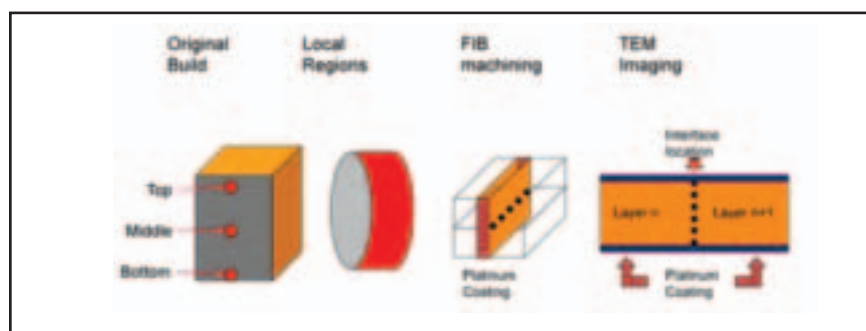


Fig. 4 — Schematic illustration of steps to prepare TEM samples from builds made with UAM. Samples were taken along interfaces at various heights (top, middle, and bottom) of the build. First, optical microscopy samples were prepared to select the regions of interest. In the next step, the sample was transferred to FIB instrument. Then, an interface of interest was selected, and a rectangular region on either side of the interface was coated with platinum. After this step, the focused ion beam machining was made on either side of the coated region. This leads to a thin film sample that contains the bonded interface. In this schematic representation, the n and $n + 1$ correspond to the successive tapes during the UAM processing.

Table 2 — Shear Test Results, Base Metal: Al 3003-H18 USS Is 110 MPa

Sample	Force (N)	Area (mm^2)	USS (MPa)	% of BM
1	5089	81.6	62.4	56.7
2	4395	80.5	54.6	49.6
3	8830	215	41.1	37.4
4	11387	216	52.6	47.8
		Average	52.7	47.9
		Standard Deviation	8.78	7.9
		Stdev/Avg	0.167	

Table 3 — Transverse Tensile Tests, Base Metal: Al 3003-H18 UTS Is 200 MPa

Sample	Force (N)	Area (mm^2)	UTTS (MPa)	% of BM
1	907	31.9	28.4	14.2
2	979	31.4	31.1	15.6
3	930	32.4	28.7	14.4
4	1010	31.4	32.1	16.1
5	859	33.5	25.7	12.9
6	601	31.4	19.1	9.6
7	1080	32.4	33.3	16.7
		Average	28.3	14.2
		Standard Deviation	4.81	2.4
		Stdev/Avg	0.170	

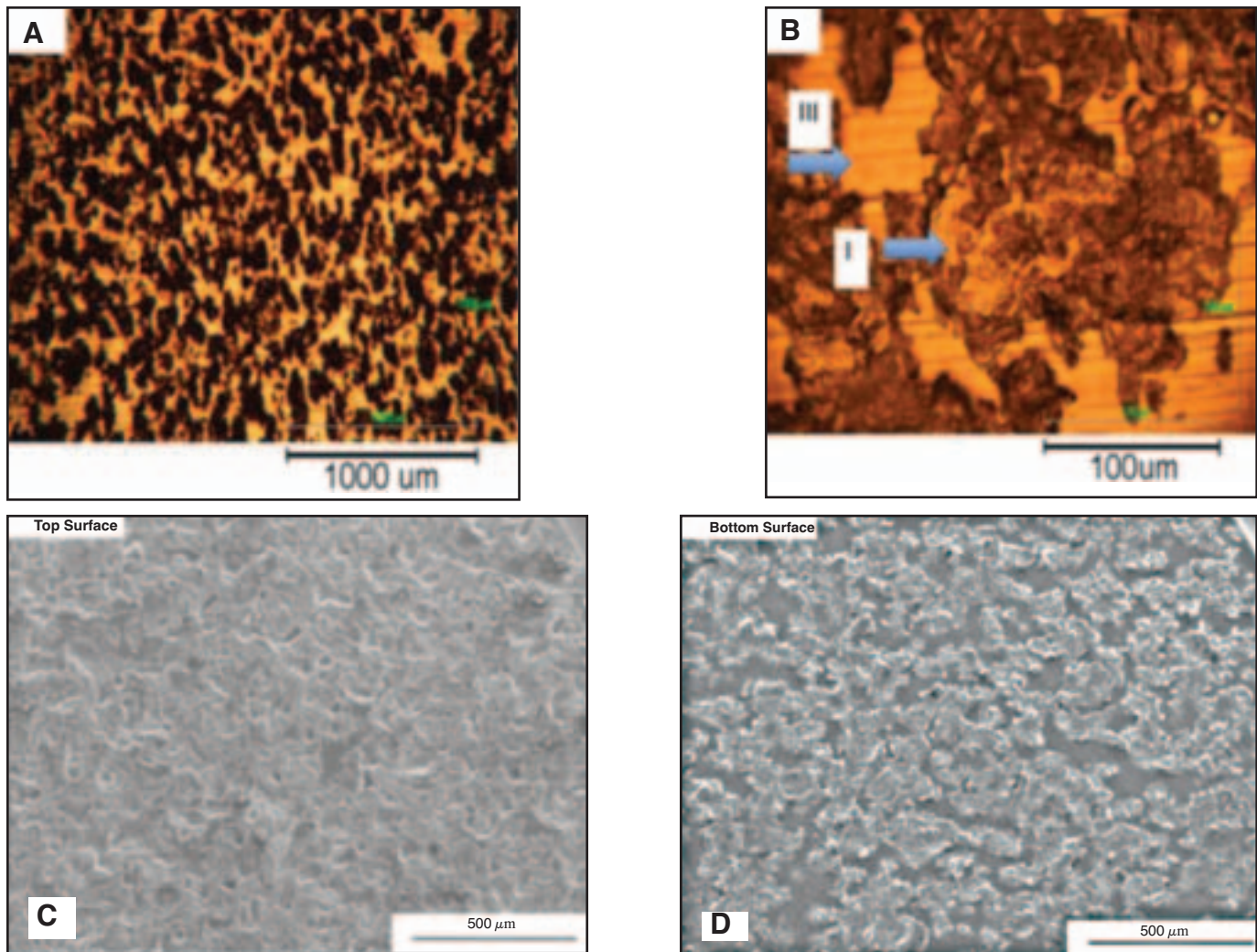


Fig. 5 — Fracture surface image analyses of transverse tensile test samples. A — Low-magnification optical image; B — high-magnification optical image showing regions I and III after processing. Region I is well bonded material with recrystallization across the interface. Region II is deep valleys carved by the sonotrode during the previous pass (not shown). Region III material is directly opposite Region II and is unaffected during the UAM process; C — SEM image of the top surface of the tape; D — SEM image of the bottom surface of the tape; and the featureless gray regions are Region III material.

area. It is important to note that the process parameters used here may not be optimum and are considered as the starting point for this and future research. Details of the peel test instrument and technique have been covered extensively by other researchers (Refs. 19–21).

Mechanical Property Testing

Previous mechanical strength studies on

UAM samples focused on peel tests (Refs. 1, 2, 4, 6, 22–24). Peel tests, while useful for comparison between parameter sets and other UAM samples, are primarily used for measuring adhesive strength of tape, glue, or other bonded surfaces and do not provide strength values useful for the design of bulk UAM parts. In order to be utilized as an additive manufacturing process, bulk mechanical strengths such as ultimate shear and tensile strengths must be known

for design of UAM samples. To date, there has been no reported research on such bulk strength properties. In order to obtain bulk strength properties of the UAM matrix, three types of samples were made: lap shear, transverse tensile, and longitudinal tensile. The geometries of these test specimens are presented — Fig. 2. The shear specimens were built such that the tape interfaces were along the shear plane. Shear tests were conducted using a specialized shear jig and a compressive load with an average displacement rate of 0.28 mm/s.

Initial shear test specimens had a reduced interface area to ensure failure below the 5000-lb machine capability. Initial estimates for strength assumed the shear strength for UAM specimens would be approximately 75% of the bulk material. As testing revealed, the shear strength was much lower than anticipated, and later samples were not prepared with a reduced interface area. The transverse tensile specimens were built such that the

Table 4 — Longitudinal Tensile Test Results, Base Metal: Al 3003-H18 UTS Is 200 MPa

Sample	Force (N)	Area (mm ²)	ULTS (MPa)	% of BM
1	2630	11.71	225	112.5
2	2900	12.21	238	119.0
3	2880	12.03	240	120.0
4	2870	12.13	237	118.5
5	2790	11.95	233	116.5
		Average	234	117.0
		Standard Deviation	5.89	2.9
		Stdev/Avg	0.025	

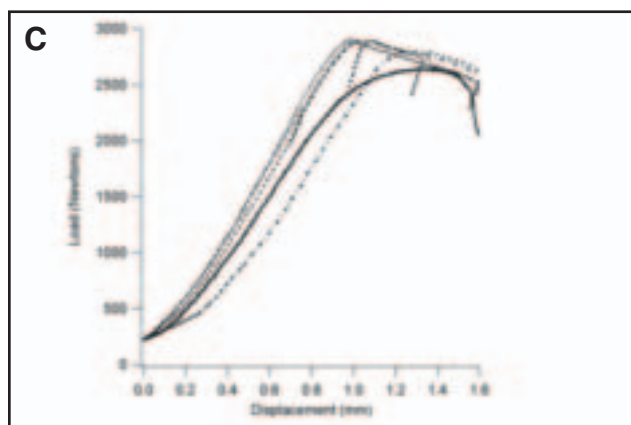
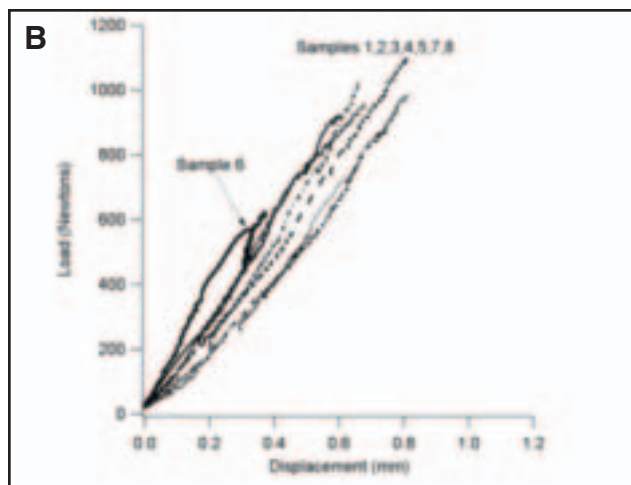
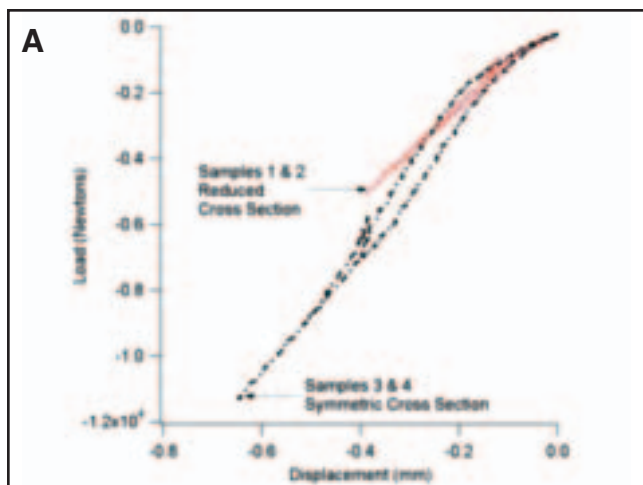


Fig. 6 — Measured load vs. displacement curves. A — Shear tests with symmetric and reduced cross sections; B — transverse tensile tests; C — longitudinal tensile tests.

tape interfaces were perpendicular to the applied axial force. Transverse tensile tests were conducted using specialized specimen shoulder grips with an average displacement rate of 0.32 mm/s. Longitudinal tensile specimens were built with tape interfaces parallel to the applied axial force and were tested using pinned grips with an average displacement rate of 0.52 mm/s.

For all tests, samples were placed in a universal tension/compression testing frame and were stressed until failure. The applied force was recorded using a tension/compression load cell and frame actuator displacement with an integrated linear variable differential transformer (LVDT). Maximum loads were used to obtain ultimate stresses, and the shape of the force-displacement plots was used to help characterize specimen failures. Because the integrated LVDT measures the testing frame actuator displacement, all displacement data includes displacement generated within the load train as well as the specimen. For this reason, the shape of the force-displacement plots can only be used to determine if a given sample failed in a brittle or ductile mode through qualitative analysis. However, this cannot be used to calculate specimen strain or related properties such as the elastic modulus. After the mechanical testing, the fracture surfaces of the shear and transverse tensile samples were examined with optical and scanning electron microscopy (SEM).

(Ref. 25). With linear intercept analyses, the LWD was measured as a function of distance in a direction perpendicular to the metallic tape layers. Grayscale image threshold values (0 to 60) were kept constant to delineate the void areas in all these images. A typical optical image before and after threshold processing demonstrates the effectiveness of delineating the voids between layers — Fig. 3A, B.

For the microhardness testing, a Leco AMH-43 machine was used to create a 200 × 20 map of hardness indents with a diamond indenter. The measurements were made with 25-g load and a 13-s dwell time, and spacing between the hardness indents was 150 μm in both directions. The coordinates of the indents were designed to sample the solid matrix regions away from interfaces. Hardness measurements were made on tapes that were not ultrasonically consolidated in the same orientation, as a reference point.

Analytical Electron Microscopy

In order to examine the grain structure and morphology in specific locations (bottom, middle, and top regions of the build) through transmission electron microscopy (TEM), the samples were prepared using a FEI Helios dual-beam focused ion beam (FIB) microscope. The samples were prepared from cross sections perpendicular to the travel direction along interfaces with apparent good bonding. The FIB

Optical Microscopy and Hardness Mapping

Optical metallographic samples were prepared using standard metallographic techniques. The samples were prepared from cross sections perpendicular to the travel direction. Five optical images at 10× magnification were taken from different locations within the build. Each image corresponded to 1111 by 833 μm, containing five interfaces. These microscopy images were analyzed with the public domain ImageJ software program

Table 5 — Linear Weld Density (%) from Optical Micrographs Taken from Random Locations within the Build

Image Number	Interface	1	2	3	4	5	Average	Standard Deviation
1		49.5	86.2	74.7	91.1	48.2	69.9	20.2
2		70.4	74.1	61.9	88.1	51	69.1	13.8
3		69.5	59.6	67.5			65.5	5.2
4		53.1	65.7	52.2	55.2	46.7	54.6	7.0
5		34.2	65.6	68.1	91.6	75.2	66.9	20.9
	Overall						65.2	15.3

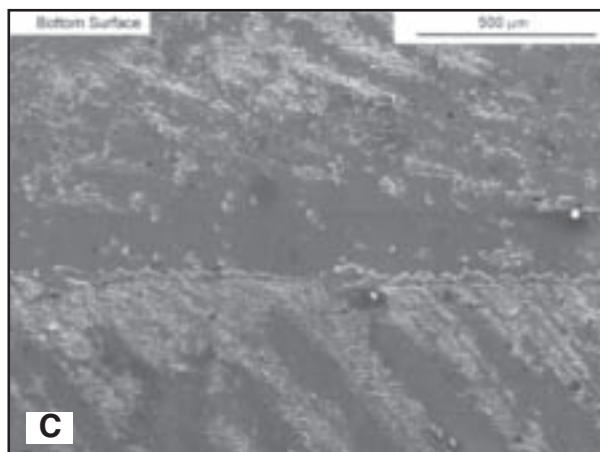
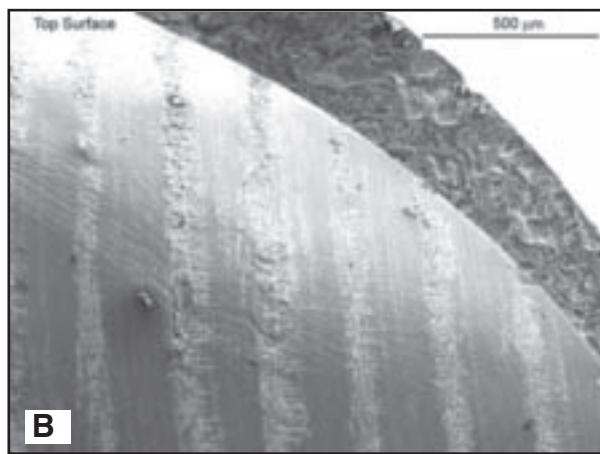
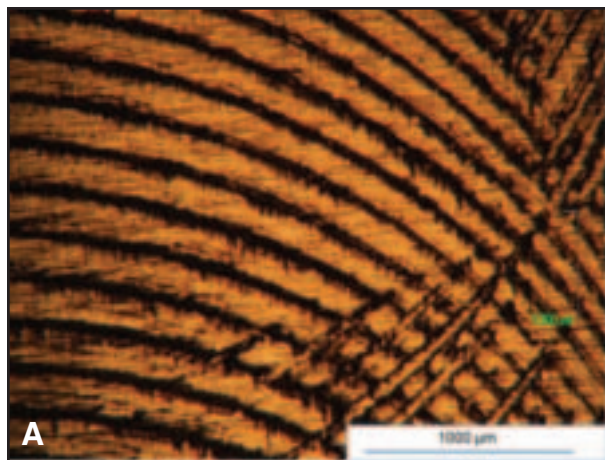


Fig. 7 — Fracture surface analyses of transverse tensile test 6. A — Optical image showing crosshatching from the milling pass; B — SEM image of the top surface of the tape containing fractured regions. It is apparent all bonding occurred in the light-colored regions, less than half of the available surface area; C — SEM image of the bottom surface of the tape containing fractured regions. It is apparent all bonding occurred in the light-colored regions, less than half of the available surface area.

contains both an electron beam as well as an ion beam that can be used for imaging. The electron beam is a standard secondary electron beam, which can be used to image topological difference but does not reveal grain structure in unetched aluminum alloys. The ion beam was used to image the grain structure of the material with contrast differences arising from gallium ion channeling contrast. To create TEM foils, platinum is deposited over the region of interest to protect the foil surface from Ga+ implantation during milling. Trenches are then milled on both sides of the platinum to create the foil. The sample is then bonded to an omniprobe needle also using platinum. The sides of the foil are then milled to create a free-standing foil. Once the sample is cut free, it is lifted out using the omniprobe needle and welded to a copper grid using platinum. Once the sample is welded to the grid, it is thinned using ion milling and a series of various apertures at 30 kV. The steps used in making the samples are schematically illustrated in Fig. 4. Finally, the samples were then examined using a FEI Tecnai F20 operated in STEM mode.

Results and Discussions

Mechanical Properties

The original mechanical properties of Al 3003-H18 alloys are as follows: The ultimate tensile strength (UTS) is 200 MPa, the yield strength (YS) is 186 MPa, and the ultimate shear strength (USS) is 110 MPa (Ref. 18). The mechanical property data from this research program are summarized in Tables 2–4. All shear tests resulted in a linear force-displacement relationship, indicating samples failed in a macro-level brittle fracture mode. As shown in Table 2, an average USS of 52.7 MPa with a standard deviation of 8.78 MPa was found. The average USS was approximately 48% of that of the solid base material. The results from the transverse

tensile tests are shown in Table 3. The average ultimate transverse tensile strength (UTTS) was 28 MPa, approximately 15% of the tensile strength of solid base material. Standard deviation for UTTS was 4.57 MPa.

To understand the reduced strength of the transverse tensile test samples, the fracture surfaces were characterized using optical and scanning electron microscopy. The fracture surfaces from the samples from 1 to 5, as well as samples 7 and 8, share a similar fracture surface — Fig. 5. These images indicate that the interface regions have many small speckled-like features dispersed throughout the bond area. This feature is due to small areas of bonded material (marked as I in Fig. 5A) mixed with small areas of unaffected material (marked as III in Fig. 5B). In order to make sure the Region I (Fig. 5B) is a true bond, the fracture surfaces from either sides of the fracture were characterized with scanning electron microscopy (Fig. 5C, D). Scanning electron microscopy showed that the fracture surfaces do show localized ductile failure with typical microvoid coalescence features. This is irrespective of the fact that the load-displacement curves do not show appreciable macro level ductility. These observations proved that the ultrasonic additive manufacturing did not reduce the inherent ductility of the material; however, on a macro scale, the material behaved in a brittle fashion due to the voids. The lack of a yield point and hardening region is related to premature brittle fracture caused by the voids.

Transverse tensile samples behaved similar to the shear samples, as indicated by the

linear force-displacement plots — Fig. 6A, B. From Fig. 6B, sample 6 is considered to be an outlier, as seen by its much lower failure force when compared to the other samples. Upon examination, the fracture surface of the sample 6 showed interesting features that were different from the other samples inspected — Fig. 7A. Optical microscopy showed trenches and ridges, which are typical of surfaces created by a milling operation (Ref. 7). Furthermore, scanning electron microscopy showed that the bonds have formed along these ridges and have failed again by ductile mode — Fig. 7B, C. Cursory evaluation of the above fracture morphology may be puzzling; however, this phenomenon may be explained. During the UAM process, at frequent intervals a milling operation is performed to achieve a flat surface to ensure dimensional accuracy of the finished part. In sample 6, the failure occurred at one such milled interface. The fracture surface showed that the area fraction of the bonded region was small compared to unbonded regions, likely the rea-

son for the premature failure of this sample. All of the samples tested had this flat pass within them; however, only sample 6 failed in this manner. Because it is not known why the other samples did not fail at this location, it is believed that sample 6 does not give a true representation of UAM bond tensile strength and is also excluded in statistical analysis. The sensitivity of surface roughness on the bond quality has been addressed by previous researchers (Refs. 7, 22) by relating the surface roughness of the sonotrode to changes in linear weld density.

Unlike the other UAM samples, the longitudinal tensile samples (Table 4) exhibited a substantial plastic yielding region after the linear elastic region — Fig. 6C. This is more typical of aluminum alloys and indicates that failure occurred in a ductile mode. All tested samples exhibited a higher than expected tensile strength. The average ultimate longitudinal tensile strength (ULTS) was 234 MPa, 17% more than the original Al 3003-H18 tape based on published properties (Ref. 18). This is a departure from both the transverse tensile samples and shear samples previously tested in which the failure stresses were significantly lower than the Al 3003-H18 tape based on published properties (Ref. 18). In this orientation, no drop in tensile strength was expected as the load was transmitted along the solid tapes as opposed to across the interfaces between them. However, the increase in strength above the base material was not expected and further explanation of this phenomenon is required.

Microstructure and Mechanical Heterogeneity

To rationalize the reduction in mechanical properties in the transverse loading condition, the LWD of the builds in different regions were analyzed. A typical data set of linear void density (inverse of LWD) is shown in Fig. 8. The image analyses show the LWD can vary from 35 to 99%, depending on the interface. The average LWD of all the images analyzed was found to be $65.2 \pm 15.3\%$, (Table 5). Image analyses of optical micrographs of the fracture surface of the transverse tensile samples (Fig. 5) yielded $66 \pm 2\%$ bonded area. In Fig. 5D, it is clear the voided regions are random in nature. In stereological terms, randomly placed line segments in cross-sectional images are proportional to an objects area in a 2-D plane (Ref. 26). However, in the current study, only one cross-sectional plane was used. This prevents the conclusion that LWD is directly related to area density of properly bonded material in UAM builds, despite the averages being comparable. With additional angular cross sections and more samples, it may be possible to confirm a possible

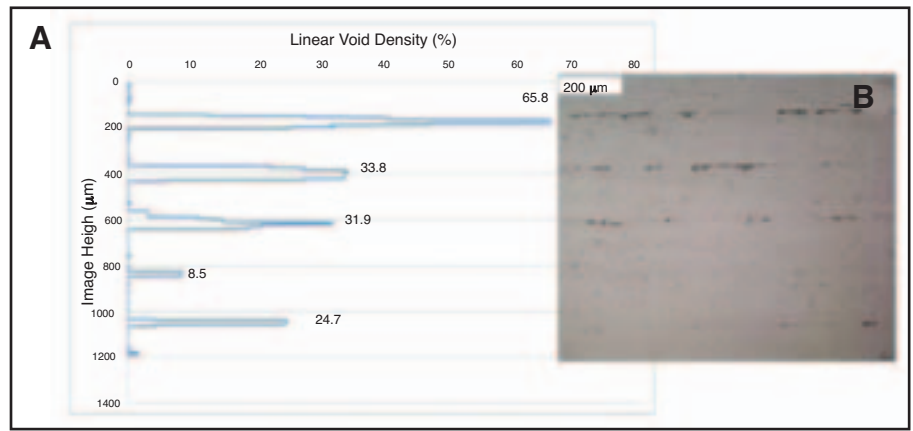


Fig. 8 — A — Plot of linear void density (LVD) vs. five interfaces; B — the corresponding optical image number 5. The LVD point for each interface was taken as the high point and is shown. Linear void density is the inverse of linear weld density.

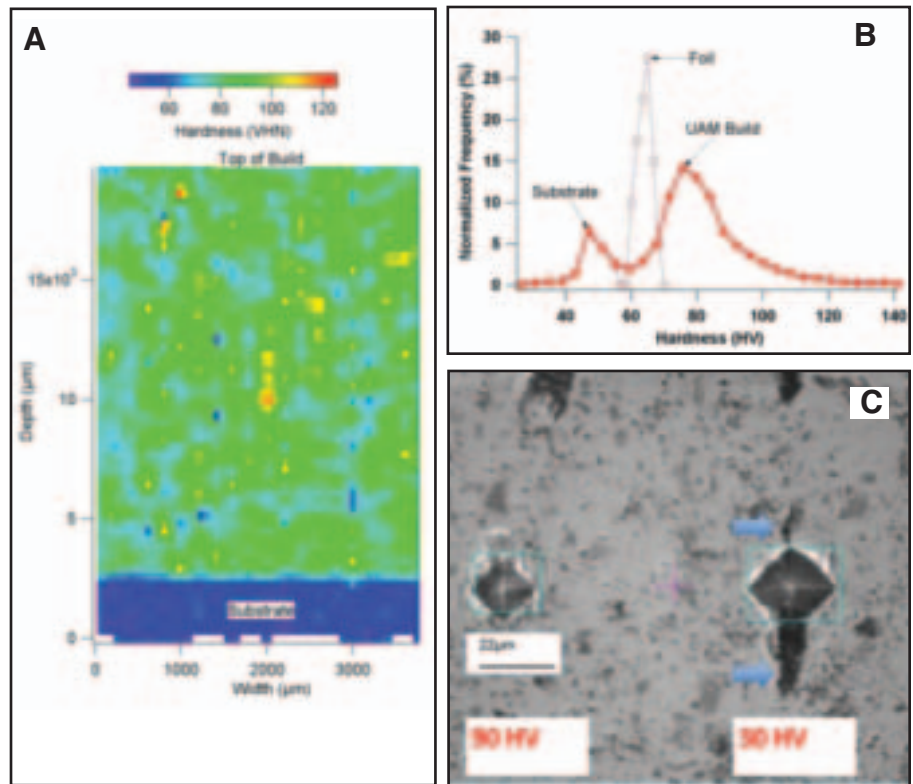


Fig. 9 — Microhardness plot of a UAM build. A — The map was 200 indents tall by 20 indents wide, with the softer substrate at the bottom. No gradient in hardness (either from bottom to top of build or left to right of build) was observed. This indicates later passes have minimal effects on the hardness of previously deposited layers; B — histogram showing bimodal hardness distribution with the UAM build foils significantly harder than the substrate. The hardness of unconsolidated foils is also overlaid on same plot and is below the peak hardness of the UAM build; C — optical image showing a high hardness foil indent on left (90 HV) next to a weaker interface indent on the right (30 HV). Interface areas with voids or defects caused by insufficient material flow to fill in grooves cut by sonotrode during previous pass had lower hardness.

one-to-one relationship. Regions with lower amounts of bonded area within the build are expected to reduce the transverse and shear strength significantly. This hypothesis is consistent with the conclusions made by previous researchers that linear weld density is a good measure of UAM bond quality.

The mechanical properties measured along longitudinal sections showed a 17%

increase in ULTS compared to that of the original Al 3003-H18 tape materials. In order to rationalize this increase in strength, hardness mapping was performed on the UAM builds. The map shows a soft substrate and UAM build regions with large variations in hardness — Fig. 9A. The hardness data were analyzed in terms of frequency distribution — Fig. 9B. This graph also shows the hardness

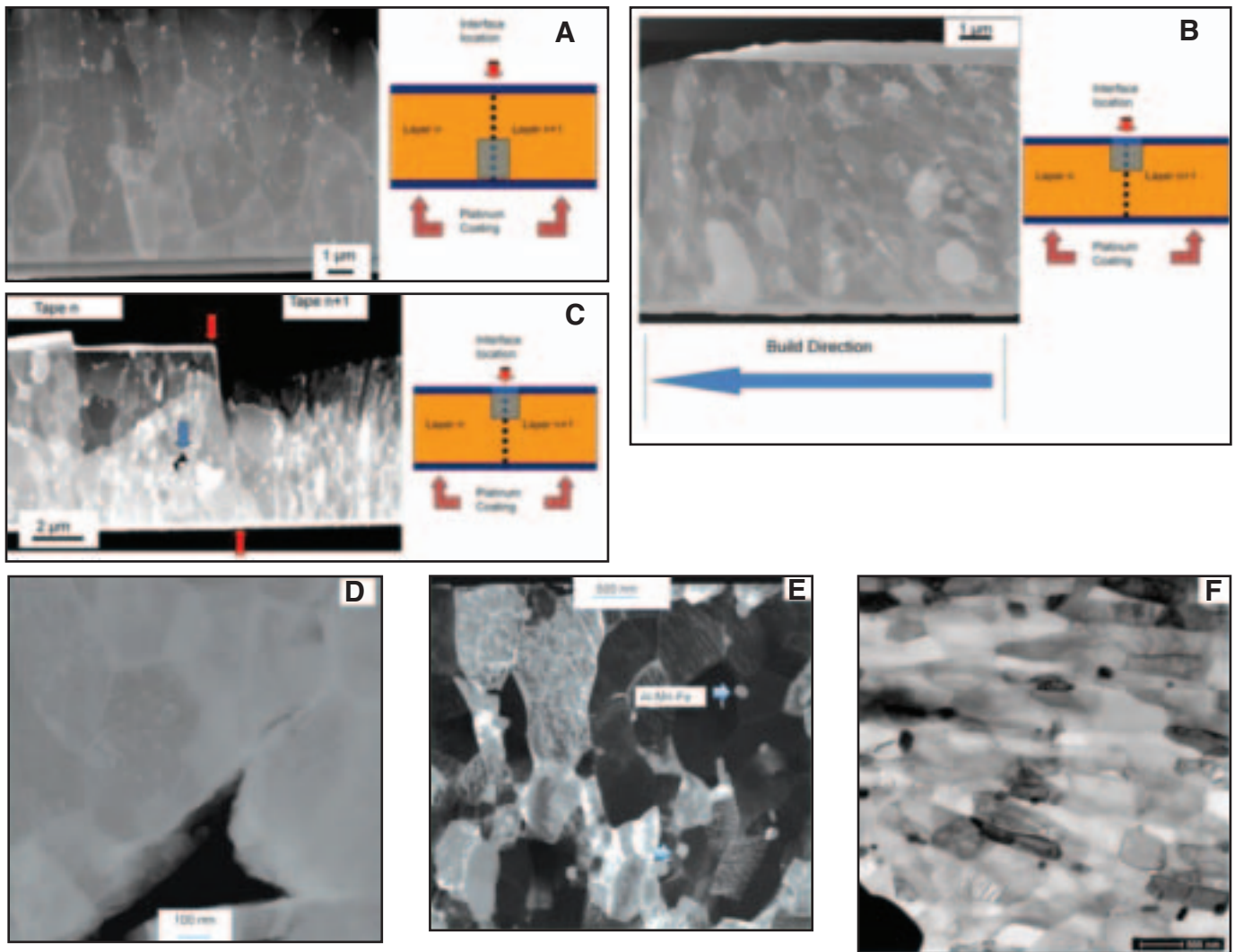


Fig. 10 — Six TEM images. A — Bright field TEM image taken from an interface location with apparent good bonding. The interface cannot be determined easily, indicating potential recrystallization across the interface. Small, white Al-Mn-Fe intermetallics can be seen here; B — another interface location again showing the difficulty in discerning the bond line; C — a third interface location where the bond line can be determined, as pointed out by the red arrows. The blue arrow points to a small void that appears to have migrated from the interface into the bulk of the material; D — high-magnification bright field image of the void in C; E — dark field image showing the high levels of dislocations within the grains and the Al-Mn-Fe intermetallic particles; F — bright field image of the original foil before consolidation. The as-rolled structure is pancake-like grains with some dislocations present. Dislocation content significantly lower than that observed after UAM processing.

distribution from the original Al 3003-H18 foils, which had an average hardness of 64.5 ± 2.7 HV. The UAM build had an average hardness of 73.7 ± 1.9 HV. The data show that the UAM builds are indeed harder than the stock foils and provide a qualitative explanation of the increase in ULTS. Careful analyses of hardness indents in certain regions also showed interesting features — Fig. 9C. In one region, a small indent showing high hardness was right next to a large indent showing low hardness. This low hardness was associated with a large planar defect (marked by arrows). Although the weakened regions may be explained with the presence of unbonded areas, it is necessary to evaluate the hardened regions through detailed microstructure characterization.

Transmission electron microscope samples from the interfaces from the bot-

tom (near substrate), middle, and top regions of the build were extracted through FIB machining. The electron microscopy images are presented — Fig. 10A–E. The microstructure of the original foil is also provided for comparison — Fig. 10F. Interestingly, the microscopy images from the bottom (Fig. 10A) and middle (Fig. 10B) regions failed to show any sharp interface region indicating the formation of a metallurgical solid-state bonding. The grains were equiaxed in nature, quite different from that of elongated grains of the original Al 3003-H18 tapes — Fig. 10F. This suggests that the bond formation may be associated with recrystallization. In addition to the equiaxed grains, fine Al-Mn-Fe-based intermetallics were observed in the samples along the grain boundaries and within the matrix grains. These intermetallics are found in the original Al 3003-

H18 tapes and do not appear to be affected by the UAM process. The interface microstructure (Fig. 10C) from the top region showed interesting features. The original interface location can be inferred from the sudden change in the grain structure. The microstructure in the $(n + 1)^{\text{th}}$ tape shows the original pancake structure, which transitions sharply to a coarse and recrystallized grain structure close to the original interface location. The microstructure from the n^{th} layer does not show any pancake structure, rather more recrystallized structure. Moreover, a region of grain boundary decohesion was also observed. This grain boundary decohesion was also confirmed with high-magnification analyses — Fig. 10D. A survey of many samples from different regions also showed the interface regions contained fine recrystallized grains (< 500

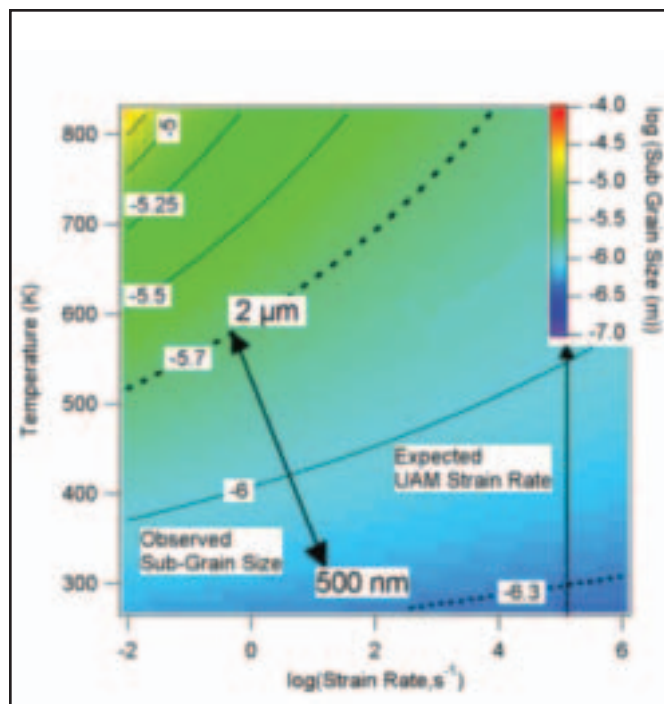
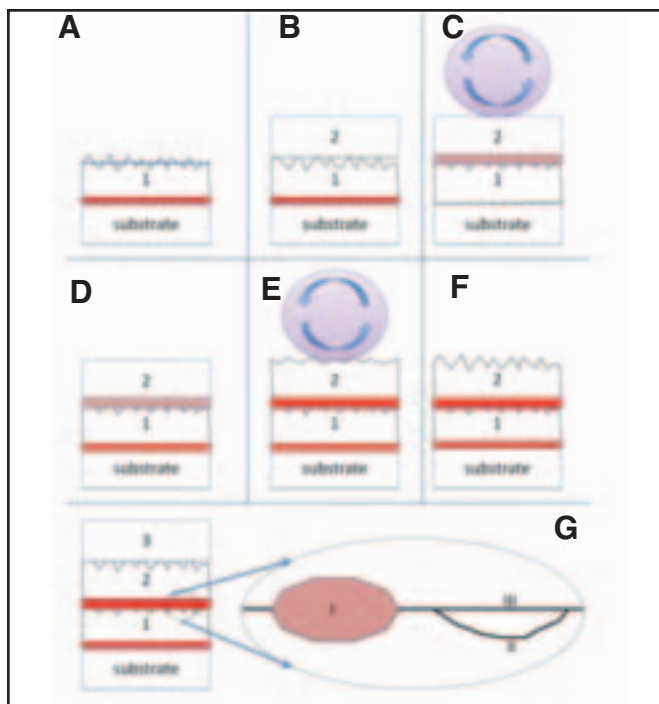


Fig. 11 — Schematic representation of the UAM process highlighting the various stages. A — Beginning of new layer, top of previous layer textured by sonotrode during previous layer bonding. B — New layer, 2, placed by feeding mechanism in front of sonotrode; C — sonotrode tacks the new layer down, generating frictional heat and forming a weak bond; D — new layer tacked down, many residual voids present; E — sonotrode passes again for welding pass, deforming the top surface as it passes; F — layer 2 attached, some voids are still present between layers 1 and 2; G — third layer ready to be added. Enlargement of bond interface showing the three regions. Region I is well-bonded material, Region II is valleys carved by sonotrode, and Region III is untouched material.

Fig. 12 — A contour plot estimating the final grain size using the Zener-Holloman parameter. The numbered, curved lines represent the possible combinations of temperature and strain rate to achieve the same grain size. Dashed lines represent the range of grain sizes found along UAM interfaces. The vertical line is the calculated strain rate derived from Equations 3–6.

nm) with relatively low dislocation density and coarse grains (500 nm to 2 μm) with relatively high dislocation density as shown by dark field microscopy — Fig. 10E. The original foil, before consolidation, shows (Fig. 10F) pancake-like grains, as expected from as-rolled material. Dislocations were present, though a much lower concentration than in the grains along interfaces after UAM processing.

Discussion on Process-Structure-Property Correlations

In order to understand the interface microstructure, it is important to review the steps involved in the UAM process, shown schematically in Fig. 11. In Fig. 11A, a first layer has been bonded to the substrate, with the top of this layer left in a rough condition after the sonotrode rolled over it. When the next layer is applied, the bottom of the new layer is relatively flat, creating an interface between a smooth surface and a rough surface — Fig. 11B. When the sonotrode comes directly on top of the interface during the tacking pass, the relative motion between the two layers creates frictional and deformational heating and partially collapses asperities

— Fig. 11C. This results in a weak bond between the layers, with many voids as shown in Fig. 11D. During the welding pass, more ultrasonic energy (higher forces and amplitude of vibration) is used to finish the bond — Fig. 11E. Some residual voids remain, as shown in Fig. 11F.

The final microstructure at the interface can be summarized to consist of three regions as shown in Fig. 11G. During the welding of the previous layer, the top surface of each foil interacts with the sonotrode and becomes rough. This rough surface becomes the bottom of the following interface. Where peaks occurred along the rough surface, contact was made with the next foil and a bond resulted (Region I). This region constitutes recrystallized microstructure (500 nm to 2 μm) across the interface and has good metallurgical bonding. It is believed these peaks are brought into contact with the new foil layer sufficient strain energy, temperature, and forces exist to force dynamic recrystallization. However, where valleys occurred due to the sonotrode texture, Region II, they were often too deep to make contact with the next layer being added. This resulted in voids along the interfaces and created the Region III mate-

rial on the foil directly above it. Region III is the unaffected original foil surface that has not been touched by either the sonotrode or the foil layer beneath it. Region III was only found on the top surface of the interface. Region II material was directly opposite and the cause of Region III material. In this study, focus was given to understand the mechanism of the grain structure evolution in Region I. Based on the microstructure from Fig. 10A–C and E, we can conclude that the original pancake grain structure was modified to form sub grains with sizes ranging from 500 nm to 2 μm with different levels of dislocation density. To understand this reduction in grain size, we assume this process is similar to that of hot working of aluminum alloys. The subgrain size (d_{sub} in μm) during hot working can be related to Zener-Holloman (Z_h) parameter and peak temperature (T_p) achieved during hot working (Refs. 27, 28).

$$d_{sub} = [-0.60 + 0.08 \log(Z_h)]^{-1} \quad (1)$$

Equation 1 has been used to estimate the grain size in both friction and friction stir welding. The Zener and Hollomon (Z_h) parameter has been estimated for

aluminum alloys as a function of strain rate ($\dot{\epsilon}$ in s^{-1}) and peak temperature (T_p) (Ref. 29).

$$Z_h = \epsilon \times \exp\left[\frac{18,772}{T_p}\right] \quad (2)$$

In order to understand the subgrain structure in UAM process, Equation 2 was used. The strain rate during ultrasonic additive manufacturing is calculated using the following approximation. The total displacement due to the plastic deformation, a thin slab of material under the horn, can be taken as the horn amplitude, i.e., ($\Delta d = 26 \times 10^{-6}$ m). This assumes there is no slippage of the interface material. The asperity height is estimated as the peak-to-peak height of the tape surface. This surface is assumed to be a negative image of the sonotrode texture, which has a value of 7×10^{-6} m, as reported by Johnson (Ref. 7). Thus, the peak-to-peak height of the average asperity is 14×10^{-6} m. Furthermore, the height of the asperities is assumed to have negligible change with respect to time. With these assumptions, displacement of the bonded regions with respect to time can be given by the expression:

$$d(t) = 26 \times 10^{-6} \times \sin(2\pi \times 20,000 \times t) \quad (3)$$

Asperity velocity is calculated as the derivative of displacement with respect to time:

$$\dot{d}(t) = v(t) = 3.3 \times \cos(2\pi \times 20,000 \times t) \quad (4)$$

The shear strain of an asperity is given by the equation:

$$\gamma = \tan^{-1}\left(\frac{d(t)}{h}\right) \quad (5)$$

Shear strain rate is then found by taking the derivative of strain with respect to time as follows:

$$\begin{aligned} \dot{\gamma}(t) &= \left[\frac{1}{\left(\frac{d(t)}{h}\right)^2 + 1} \right] \times \frac{\dot{d}(t)}{h} \\ &= \left[\frac{1}{\left(\frac{d(t)}{h}\right)^2 + 1} \right] \times \frac{v(t)}{h} \quad (6) \end{aligned}$$

Over one ultrasonic cycle, an asperity will have a strain rate varying between $\pm 2.3 \times 10^5$ rad/s with an RMS value of

$\pm 1.1 \times 10^5$ rad/s. Because we do not know the peak temperatures experienced by interface regions, the subgrain sizes were evaluated as a function of peak temperature and strain rate. This is shown as a form of contour plot — Fig. 12. The calculated micro strain rate from Equation 6 results in a peak temperature of around 300 K for the 500-nm grains and a peak temperature of 900 K for the 2- μ m grains. This range of temperatures is larger than expected, but this may have been caused by the approximations in Equations 1 to 6. In Equation 6, perfect transfer of strain was assumed, no slipping between the sonotrode and the foil was accounted for. Account for slipping, the resulting strain, and therefore peak temperature required to achieve a certain grain size, would have decreased. Meanwhile, Equations 1 and 2 were developed for simple monotonous hot working conditions and not reversible strains that are experienced during UAM. Gunduz et al. (Ref. 30) estimated a local strain rate of $1 \times 10^4 s^{-1}$ at a temperature of 513 K based on vacancy calculations and the diffusion profile observed in aluminum-zinc ultrasonic welds. This work was based on finding the vacancy concentration required to reduce the melting temperature so the observed small melt region was possible at ultrasonic welding temperatures. Their result is within the range of grain size, temperatures, and strain rates studied here. Conversely, macro strain rates were studied by Gao and Doumanidis (Ref. 31) by placing a strain gauge near, but not directly beneath, the welding sonotrode. They found maximum strains of 90×10^{-6} over 0.5 s or $1.8 \times 10^{-4} s^{-1}$. This low strain rate is expected as Gao and Doumanidis measured macro strains with a strain gauge of a much larger size scale than the asperities used in Equation 6.

Recently, Johnson has proposed that the materials under reversible straining conditions may exhibit an Ultrasonic Bauschinger effect (Ref. 7). However, the interaction of these effects with heating and subgrain formation is not clear. In addition, the estimated strain rates have to be validated based on detailed finite element deformation models (Ref. 12), which considers the spatial variations as well as dynamic strain hardening or softening. The localized temperature along interfaces may be affected by the friction and rapid deformation conditions. In the current UAM process, the substrate temperature is maintained at 149°C (422 K). This heat will diffuse from the substrate to the entire build. As a result, with the progress of UAM builds, the previously welded interfaces will be subjected to an isothermal hold close to this temperature throughout the processing of the build. This isothermal hold is also

expected to induce some of the recrystallization and grain growth observed. This suggests the need for measuring the spatial and temporal variations of the temperature during the UAM process. This will be the focus of the future work (Ref. 32). The next step is to provide some directions to rationalize the measured mechanical properties. From the above discussions, it is apparent that all UAM samples will have large voids along the interfaces as well as localized hard and soft regions. The voids can be treated as embedded cracks, which cause stress concentrations that resulted in brittle fracture of the shear and transverse tensile specimens. The loading of the transverse tensile samples results in a mode I fracture, while the shear sample loading induces mode II fracture. For a given crack and load magnitude, mode I fracture loading typically exhibits the largest stress intensity factor (SIF) followed by mode II fracture (Ref. 33). Because loading is parallel to the embedded cracks in the longitudinal tensile samples, there is no SIF and the strength in this orientation was not reduced. This fracture mechanics perspective further explains why the shear and transverse tensile samples have lower than normal strengths and brittle fracture characteristics, while the longitudinal samples were not weakened by the presence of voids and instead failed with ductile characteristics. Again, the above discussion is simplistic, does not provide a predictive capability, and does not account for all transients that have been observed, such as the variations in tensile testing shown — Fig. 6. Further work is necessary to develop detailed computational models that incorporate the spatial variation of microstructure and voids and constitutive response of the bulk and interface location. To facilitate the development of constitutive properties of the interface locations, the grain size distribution along the interface has to be characterized close to the voids and away from the voids using orientation-imaging microscopy. This grain orientation and size distribution will allow us to develop multiscale models similar to the ones being developed by Ghosh (Ref. 34).

Finally, in order to overcome the deep channels carved by the sonotrode, a very high power UAM system is being developed by EWI (Ref. 17). It is believed that higher ultrasonic power input, higher amplitudes, and normal forces will increase the plastic flow at the interfaces. This should enable greater LWD, reducing the inherent stress concentrations and improving the tensile and shear strength of UAM builds. Higher plastic flows should also improve the metallurgical bonds by ensuring all of the oxides are removed from the interface.

Conclusions

The present study focused on linking microstructure and LWD to mechanical properties of ultrasonic additive manufacturing builds. Using TEM, SEM, and optical microscopy along with microhardness and tensile and shear testing, the microscopic and macroscopic properties of UAM builds were analyzed. The following was found:

1. The average shear strength of the tested UAM samples was approximately 48% of the expected 110 MPa ultimate shear strength of Al 3003-H18. The average transverse tensile strength was approximately 14% of the expected 200 MPa tensile strength of Al 3003-H18. Transverse tensile and shear testing results are indicative of bond quality alone; failure occurs before microstructure becomes significant.

2. Without optimized parameters, UAM weldments result in voids scattered throughout all interfaces. This ultimately caused the samples to fail in a low ductility manner with low strength values.

3. Image analysis of cross-sectioned samples found an average linear weld density of $67.4 \pm 16.1\%$. Image analysis of transverse tensile fracture surfaces found an average area weld density of $66 \pm 2\%$. A direct comparison between LWD and area weld density was not possible based on the sample size.

4. The average longitudinal tensile strength was approximately 117% of the expected tensile strength of Al 3003-H18. This indicates the foils were strengthened during processing and was confirmed by microhardness testing. Microhardness testing found the average hardness of the UAM foils increased almost 15%, from 64.5 ± 2.7 HV in the original foils to 73.7 ± 1.9 HV, during processing.

5. A hypothesis relating grain refinement to strain and temperature using the Zener-Hollomon parameter was developed. Microstrain rates were estimated based on operating conditions to be around 1×10^5 s⁻¹. From this and an observed grain size of 500 nm to 2 μ m, an estimated peak temperature range for the UAM process of 300 to 900 K was calculated.

Acknowledgments

The authors would like to thank the Cooperative Research Program of Edison Welding Institute for supporting this research. In addition, we thank Dr. K. Graff (EWI), Dr. M. Sriram (OSU), and Matt Short (EWI) for suggestions and fruitful discussions during preparation of the manuscript. R. M. Hahnen and M. J.

Dapino are grateful to the member organizations of the Smart Vehicle Concepts Center (www.SmartVehicleCenter.org), the National Science Foundation Industry/University Cooperative Research Program (I/UCRC), and the Smart Vehicle Concepts Graduate Fellowship Program.

References

1. Kong, C., Soar, R., and Dickens, P. 2004. Optimum process parameters for ultrasonic consolidation of 3003 aluminium. *Journal of Materials Processing Technology* 146: 181–187.
2. Kong, C., Soar, R., and Dickens, P. 2004. A model for weld strength in ultrasonically consolidated components. *Journal of Mechanical Engineering Science* 219: 83–91.
3. Yang, Y., Janaki Ram, G. D., and Stucker, B. E. 2007. An experimental determination of optimum processing parameters for Al/SiC metal matrix composites made using ultrasonic consolidation. *American Society of Mechanical Engineers* 129: 538–549.
4. Kong, C., Soar, R., and Dickens, P. 2003. Characterisation of aluminium Alloy 6061 for the ultrasonic consolidation process. *Materials Science and Engineering A* 363: 99–106.
5. Janaki Ram, J. D., Yang, Y., and Stucker, B. E. 2006. Effect of process parameters on bond formation during ultrasonic consolidation of aluminum Alloy 3003. *Journal of Manufacturing Systems* 25: 221–238.
6. George, J., and Stucker, B. E. 2006. Fabrication of lightweight structural panels through ultrasonic consolidation. *Virtual and Physical Prototyping* 1: 227–241.
7. Johnson, K. 2008. Interlaminar subgrain refinement in ultrasonic consolidation. PhD thesis, Loughborough University, Loughborough, UK.
8. Adams, B. L., Nylander, C., Aydellote, B., Ahmadi, S., Landon, C., Stucker, B. E., and Janaki Ram, G. D. 2008. Accessing the elastic-plastic properties closure by rotation and lamination. *Journal of Acta Materialia* 56: 128–139.
9. Li, D., and Soar, R. C. 2008. Plastic flow and work hardening of Al alloy matrices during ultrasonic consolidation fiber embedding process. *Materials Science and Engineering A* 498: 421–429.
10. Doumanidis, C., and Gao, Y. 2004. Mechanical modeling of ultrasonic welding. *Welding Journal* 83(4): 140-s to 146-s.
11. Janaki Ram, G. D., Robinson, C., Yang, Y., and Stucker, B. E. 2007. Use of ultrasonic consolidation for fabrication of multi-material structures. *Rapid Prototyping Journal* 13: 226–235.
12. Zhang, C., and Li, L. 2009. A coupled thermal-mechanical analysis of ultrasonic bonding mechanism. *The Minerals, Metals and Materials Society and ASM International*: 196–207.
13. Siddiq, A., and Ghassemieh, E. 2008. Thermomechanical analysis of ultrasonic welding process using thermal and acoustic softening effects. *Mechanics of Materials* 40: 982–1000.
14. Matsuoka, S., and Imai, H. 2009. Direct welding of different metals using ultrasonic vibration. *Journal of Materials Processing Technology* 209: 954–960.
15. Kong, C. Y., Soar, R. C., and Dickens, P. M. 2004. Ultrasonic consolidation for embedding SMA fibers within aluminum matrices.

Composite Structures 66: 421–427.

16. Hahnen, R. 2009. Development and characterization of NiTi joining methods and metal matrix composite transducers with embedded niti by ultrasonic consolidation. Master's thesis, The Ohio State University, Columbus, Ohio.

17. Sriraman, M. R., Babu, S. S., and Short, M. 2010. Bonding characteristics during very high power ultrasonic additive manufacturing of copper. *Scripta Materialia* 62: 560–563.

18. *Aluminum Standards and Data*. 1993. Aluminum Association.

19. White, D. 2003. Ultrasonic object consolidation. U. S. patent US 6,519,500 B1.

20. White, D., and Carmein, D. E. 2002. Ultrasonic object consolidation systems and method. U. S. patent US 6,446,349 B2.

21. White, D. 2003. Ultrasonic consolidation of aluminum tooling. *Advanced Materials and Processes*: 64, 65.

22. Li, D., and Soar, R. 2009. Influence of sonotrode texture on the performance of ultrasonic consolidation machine and the interfacial bond strength. *Journal of Materials Processing Technology* 209: 1627–1634.

23. Li, D., and Soar, R. C. 2009. Characterization of process for embedding sic fibers in Al 6061 O matrix through ultrasonic consolidation. *Journal of Engineering Materials and Technology* 131: 021016.

24. Hazlett, T. H., and Ambekar, S. M. 1970. Additional studies of interface temperature and bonding mechanisms of ultrasonic welds. *Welding Journal* 49(5): 196-s to 200-s.

25. Abramoff, M. D., Magelhaes, P. J., and Ram, S. J. 2004. Image processing with ImageJ. *Biophotonics International* 11(7): 36–42.

26. Mouton, P. R. 2002. *Principles and practices of unbiased stereology, an introduction for bioscientists*. John Hopkins University Press.

27. Frigaard, O., Grong, O., and Midling, O. T. 2001. A process model for friction stir welding of age hardenable alloys. *Metallurgical and Materials Transactions A32*: 1189–1200.

28. Midling, O. T., and Grong, O. 1994. A process model for the friction welding of Al-Mg-Si alloys and Al-SiC metal-matrix composites: HAZ temperature and strain-rate distribution. *Acta Metall. Mater* 42: 1595–1609.

29. Grong, O. 1997. *Metallurgical Modeling of Welding*, 2nd ed. The Institute of Materials. Materials Modeling Series.

30. Gunduz, I. E., Ando, T., Shattuck, E., Wang, P. Y., and Doumandis, C. 2005. Enhanced diffusion and phase transformations during ultrasonic welding of zinc and aluminum. *Journal of Acta Materialia* 52: 939–943.

31. Gao, Y., and Doumanidis, C. 2002. Mechanical analysis of ultrasonic bonding for rapid prototyping. *Journal of Manufacturing Science and Engineering* 124: 426–434.

32. Schick, D. E. Submitted 2010. Transient thermal response in ultrasonic additive manufacturing of aluminum 3003. *Rapid Prototyping Journal*.

33. Dieter, G. E. 1986. *Mechanical Metallurgy*, 3d ed. McGraw Hill.

34. Ghosh, S., Bai, J., and Paquet, D. 2009. Homogenization-based continuum plasticity-damage model for ductile failure of materials containing heterogeneities. *Journal of Mechanical Physical Solids* 57: 1017–1044.

WELDING *Journal*

Guidelines for submitting electronic files

1. Platform:

Macintosh or PC accepted

2. Files accepted:

QuarkXpress, Adobe Photoshop, Adobe Illustrator, TIFF, EPS and PDF files only.

3. Color:

Send all files in as CMYK (for color) or Grayscale (for b/w).

4. Images:

Minimum resolution required for magazine printing is 300 dpi for full color artwork or grayscale at least 1000 dpi for bitmap (B&W/line art). Images and logos from Web sites are NOT usable for printing. They are low resolution images (72 dpi). Images taken with a digital camera are not acceptable unless they meet the minimum 300 dpi requirement.

5. Proof:

A proof of the images should **always** be provided.

6. Electronic File Transfer:

Files larger than 20 MB are not acceptable as an email attachment; please send it on a CD or Zip, you may also send files to the printer FTP site (a user name and password will be provided when requested)

Check list for submitting electronic files:

Colors: 4/C Grayscale B&W/line art

File Type: TIFF EPS

File sent via: DVD Zip disk CD Email

Proof supplied/faxed

CMYK images at 300 dpi or higher, B&W/line art at 1000 dpi or higher.

All color in all images set to CMYK process (not RGB)

When submitting ads, please send them to the attention of

Frank Wilson
Advertising Production Manager
American Welding Society
550 NW LeJeune Rd.
Miami, Fla. 33126